Supporting Information for "Time-Varying Internal Tides Revealed by Mooring Measurements in SWOT Cal/Val Pre-Launch Field Campaign 2019"

Tongxin Cai[1,2], Zhongxiang Zhao[1,2], Eric D'Asaro[1,2], Jinbo Wang[3],

Lee-Lueng Fu[3]

[1]Applied Physics Laboratory, University of Washington, Seattle, Washington, USA.

[2]School of Oceanography, University of Washington, Seattle, Washington, USA.

[3]Jet Propulsion Laboratory, California Institute of Technology, Pasadena, California, USA.

Contents of this file

Introduction

1. Data processing and equations

1.1. Quality control

Several steps of quality control are conducted. First, data below the surface mixed layer are selected, with a mixed layer depth of 60 m chosen for both moorings (Figure S1). Additionally, unrealistic extreme values or missing values are identified and removed. Specifically, the bottom 4510-m CTD data are excluded due to data corruption (Wang et

———

Corresponding author: T. Cai, School of Oceanography, University of Washington, 1503 NE Boat Street, Seattle, WA 98195-7940, USA (joycecai@uw.edu)

January 6, 2024, 4:43am

al., 2022), and the 261-m CTD data are disregarded due to a high level of noise observed

in the frequency spectrum analysis (Figure S4d).

1.2. Buoyancy frequency

The buoyancy frequency is defined as

$$N^2(z) = -\frac{g}{\rho_0}\frac{d\sigma(z)}{dz} \tag{1}$$

1.3. Displacement correction

The pressure measurement taken at each CTD and the configuration of the mooring

have revealed that the north mooring experienced a pull-down of approximately 300 m

due to its "slack" design. As a result, the CTDs were not precisely fixed at the intended

pressure level, resulting in slight vertical movements (Figure S3), especially in deeper

waters (beyond 1000 m). Therefore, it is essential to adjust the vertical displacement at

each depth by removing the component caused by pressure variations η_P, which we define

as follows:

$$\eta_P(z,t) = \overline{P}(z,t) - P(z,t) \tag{2}$$

Here $\overline{P}(z,t)$ is the 10-day moving-average pressure at depth z. An example of η_P is shown

in Figure S6b for the sensor at 2750 m from the north mooring. By taking account of the

small vertical motion of CTDs, we have the vertical internal tide displacement η_{tide} as

$$\eta_{tide}(z,t) = \eta_\sigma(z,t) + \eta_P(z,t) \tag{3}$$

The data from the south mooring with taut design were less affected, but it is still crucial

to apply the correction. The displacement correction at 2750 m for the north mooring is

illustrated in Figure S6.

1.4. Phase velocity

In a nonrotating fluid, the eigenvalue velocity c_n is equal to phase velocity and group velocity. If under the influence of Earth's rotation Ω, the phase velocity c_p of each mode can be calculated based on dispersion relation following (Rainville & Pinkel, 2006; Zhao, 2021)

$$c_p^n = \frac{\omega}{\sqrt{\omega^2 - f^2}} c_n \tag{4}$$

where ω is the tidal frequency in this study and f is the inertial frequency. The phase velocity c_p^n of each mode varies with ocean stratification, as it is determined by the eigenvalue velocity c_n, which is a function of the buoyancy frequency $N(z)$ and depth H. The phase velocity at each time is then projected onto each mode by addressing a least squares problem.

2. Spectrum of vertical displacement

Prominent semidiurnal signals are observed across sensors in various depth below mixed layer depth at the north mooring (Figure S4). The significance of these tidal peaks is statistically confirmed within both the 95% (dim gray) and 50% (dark gray) confidence intervals (CI). To compute the spectra, a sine multitaper method was employed, utilizing a degree of freedom (DOF) of 4. Additionally, a geometric smoothing process was applied, spanning 1/250 of the total bandwidth, to enhance spectral coherence. At the south mooring (Figure S5), the measurements obtained from the fixed CTDs below 500 meters also exhibit dominant semidiurnal signals, characterized by notable peaks of the M_2 constituent and their statistical significance. At the sensor positioned at a depth of 4395 meters (Figure S5h), near the bottom (4516 m), the vertical displacement is primar-

ily influenced by turbulence induced by currents and/or waves within the weakly-stratified bottom boundary layer (Garrett, 2003; Wunsch et al., 2004; Kunze, 2017) .

3.   Mode fitting number sensitivity analysis

Theoretical considerations of modal decomposition suggest that the number of modes employed for fitting does not significantly affect the obtained results due to the orthogonality of modes. However, practical challenges arise when performing on data sets characterized by vertical spatial gaps (Nash et al., 2005). These challenges are particularly pronounced for higher-mode signals due to their vertical structure and relatively weak magnitude, especially in scenarios where the available upper ocean data is sparse or lacks deep ocean observations (Zhao et al., 2010). Additionally, the computational burden associated with fitting a large number of modes is considerable. Consequently, determining the optimal number of modes for the decomposition process becomes imperative.

To evaluate the influence of incomplete water column coverage in mooring configurations in the campaign, we conducted a sensitivity analysis by varying the number of modes used for mode fitting. Specifically, we examined six distinct scenarios: fitting only mode 1, fitting mode 1-2, fitting mode 1-3, fitting mode 1-5, fitting mode 1-8, and fitting mode 1-10. The energy of the low-mode tide (mode 1-3) was compared across these scenarios, as depicted in Figure S7. Notably, the energy of the low-mode tide in both moorings converged when employing five or more modes for fitting. Considering the computational costs involved, it is evident that fitting the lowest five modes suffices for our analytical purposes, particularly when focusing on mode-1 and mode-2.

References

de Boyer Montégut, C., Madec, G., Fischer, A. S., Lazar, A., & Iudicone, D. (2004). Mixed layer depth over the global ocean: An examination of profile data and a profile-based climatology. *Journal of Geophysical Research: Oceans*, *109*(C12).

Garrett, C. (2003). Internal tides and ocean mixing. *Science*, *301*(5641), 1858–1859.

Kunze, E. (2017). Internal-wave-driven mixing: Global geography and budgets. *Journal of Physical Oceanography*, *47*(6), 1325–1345.

Li, Q., & Fox-Kemper, B. (2017). Assessing the effects of Langmuir turbulence on the entrainment buoyancy flux in the ocean surface boundary layer. *Journal of Physical Oceanography*, *47*(12), 2863–2886.

Nash, J. D., Alford, M. H., & Kunze, E. (2005). Estimating internal wave energy fluxes in the ocean. *Journal of Atmospheric and Oceanic Technology*, *22*(10), 1551–1570.

Rainville, L., & Pinkel, R. (2006). Propagation of low-mode internal waves through the ocean. *Journal of Physical Oceanography*, *36*(6), 1220–1236.

Wang, J., Fu, L.-L., Haines, B., Lankhorst, M., Lucas, A. J., Farrar, J. T., ... others (2022). On the Development of SWOT In Situ Calibration/Validation for Short-Wavelength Ocean Topography. *Journal of Atmospheric and Oceanic Technology*, *39*(5), 595–617.

Wunsch, C., Ferrari, R., et al. (2004). Vertical mixing, energy, and the general circulation of the oceans. *Annual Review of Fluid Mechanics*, *36*(1), 281–314.

Zhao, Z. (2021). Seasonal mode-1 M_2 internal tides from satellite altimetry. *Journal of Physical Oceanography*, *51*(9), 3015–3035.

Zhao, Z., Alford, M. H., MacKinnon, J. A., & Pinkel, R. (2010). Long-range propagation of the semidiurnal internal tide from the Hawaiian Ridge. *Journal of Physical*

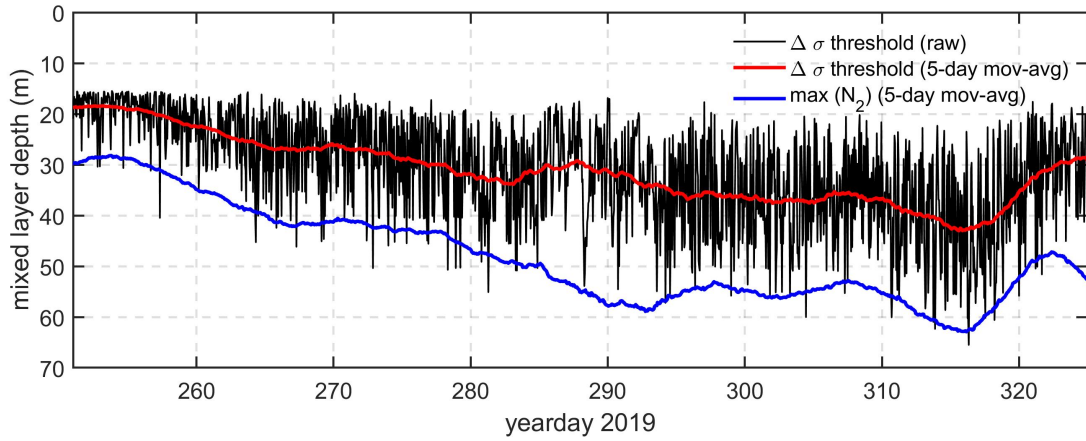*Oceanography*, *40*(4), 713–736.

Figure S1. Mixed layer depth (MLD, in unit of m) at the south mooring. Two criteria are used: $\Delta\sigma$ criteria (de Boyer Montégut et al., 2004) and maximum buoyancy frequency (N^2) criteria (Li & Fox-Kemper, 2017). The threshold of $\Delta\sigma = 0.03 kg/m^3$ and its temporal variation of MLD is plotted as a black line (raw data) and a red line (after 5-day moving averaging). The blue line represent the MLD using maximum buoyancy frequency criteria, also after 5-day moving average. Consistent deepening of the MLD is observed, starting from 25m and ending with 40m, with the maximum depth reaching 60m.

Figure S2. One-hour grided potential density σ (kg/m^3) at the south mooring (a) at upper 500 m from WireWalker Profiler and (b) 500 m - 4390 m from fixed CTDs. Colors indicate potential density σ (kg/m^3) with blue as lighter and red as denser. Black contour lines are isopycnals with constant density value. Note that there are different colorbar limits for (a) and (b).
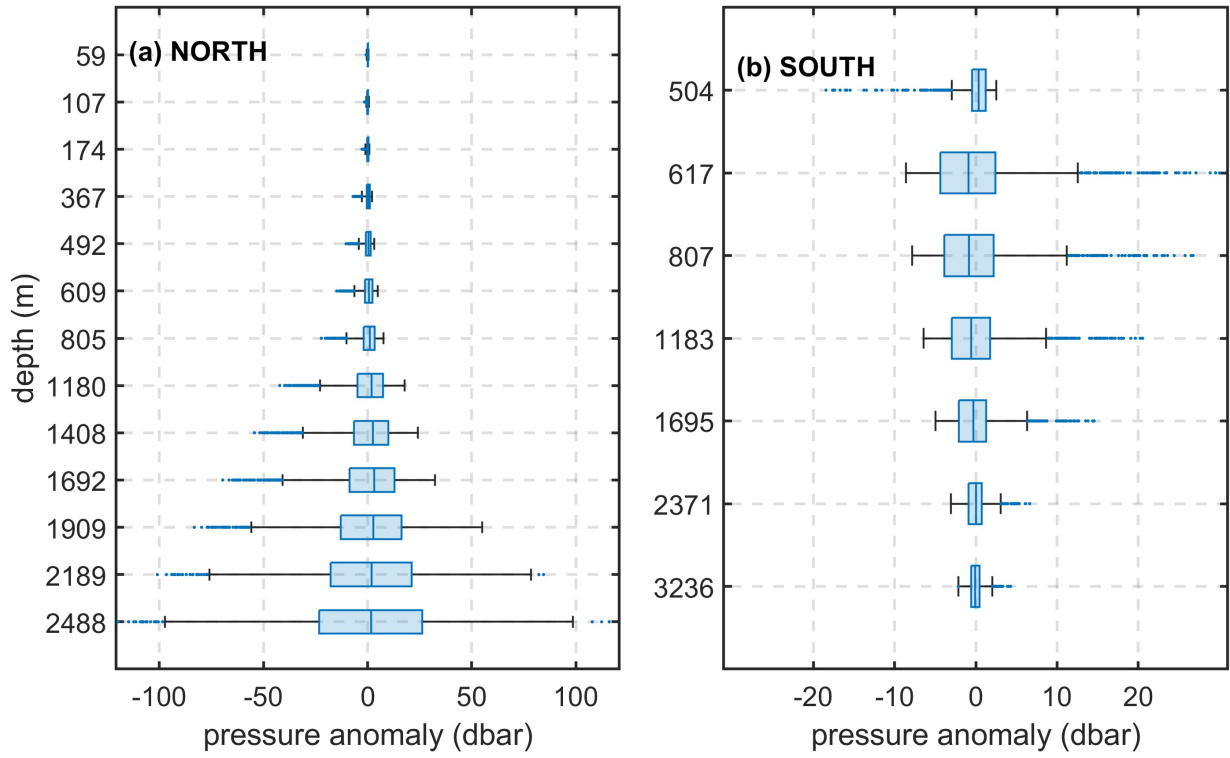
Figure S3. Box plot of pressure anomaly (dBar) of fixed CTDs from (a) the north mooring and (b) the south mooring. Due to the mooring configuration, there is large pressure variation from CTDs at the north mooring, especially in the deeper ocean. There is less effect on the south mooring.
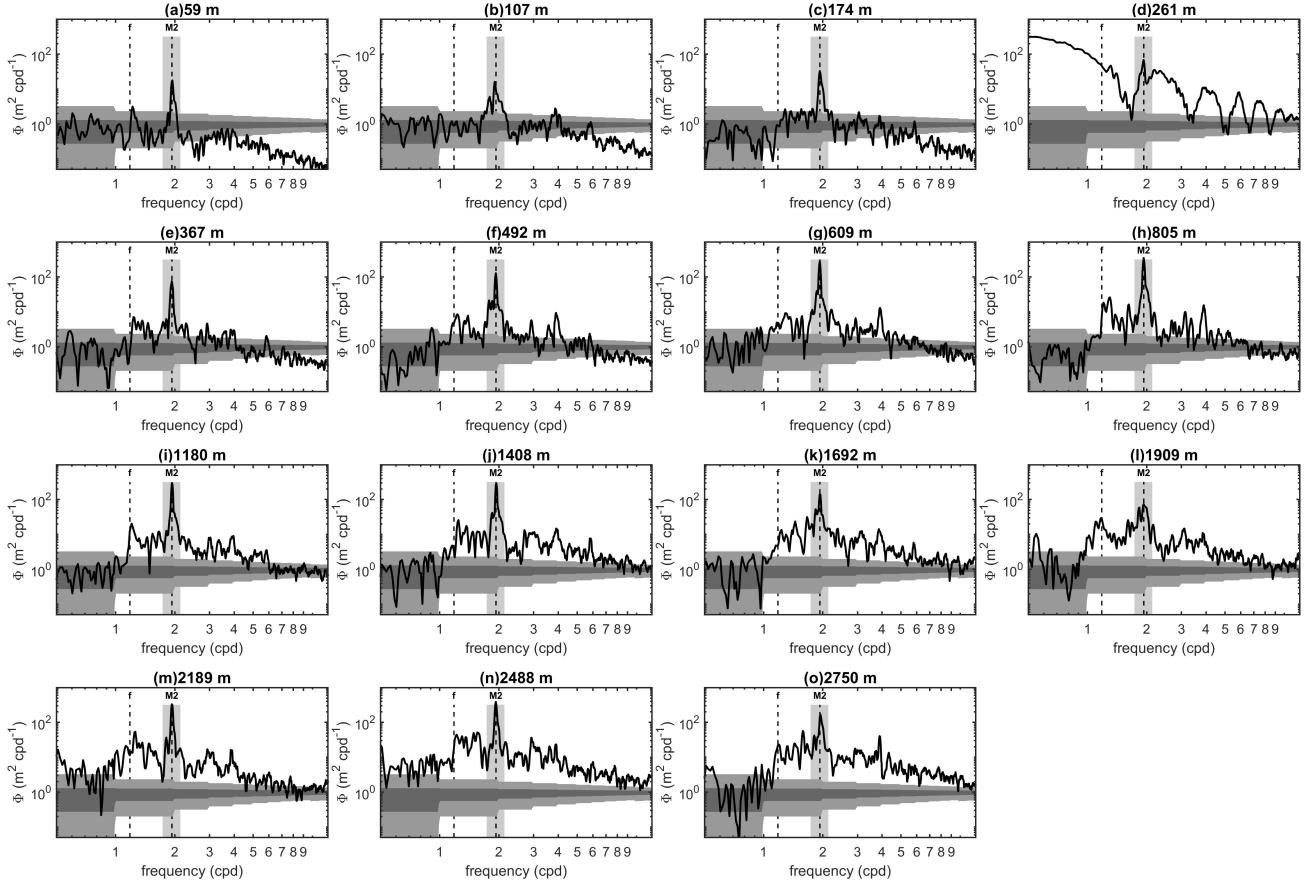
Figure S4. The spectrum of tidal displacement from every sensor at the north mooring. Dim gray are 95% Confident Interval (CI) and dark gray are 50% CI. The semidiurnal band used for filtering are shown in light gray. The two dashed lines indicate the Coriolis f and M_2 frequency. (d) The sensor at 261 m shows high level of noise and uncertainty. Therefore, it is disregard in the tidal analysis.
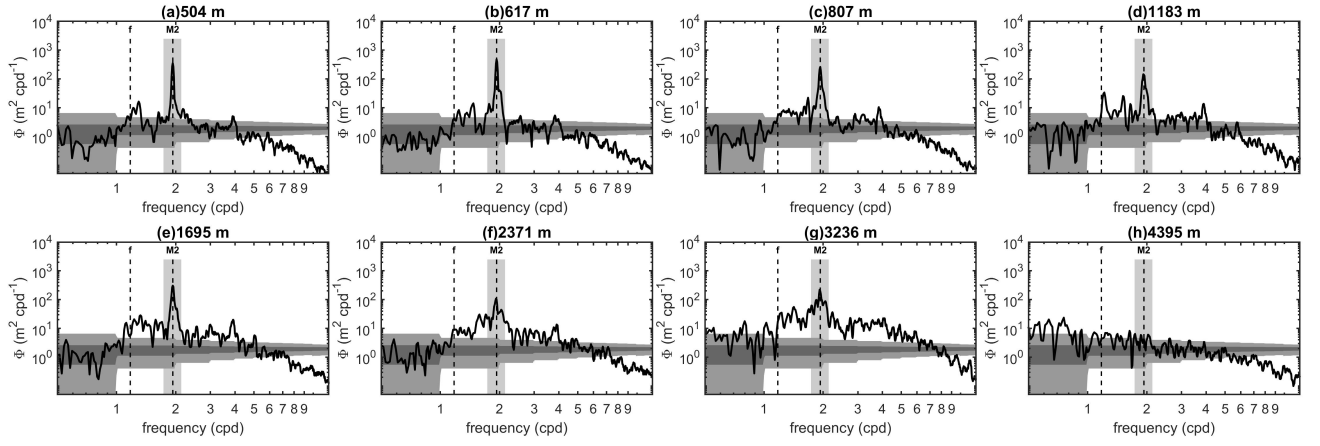
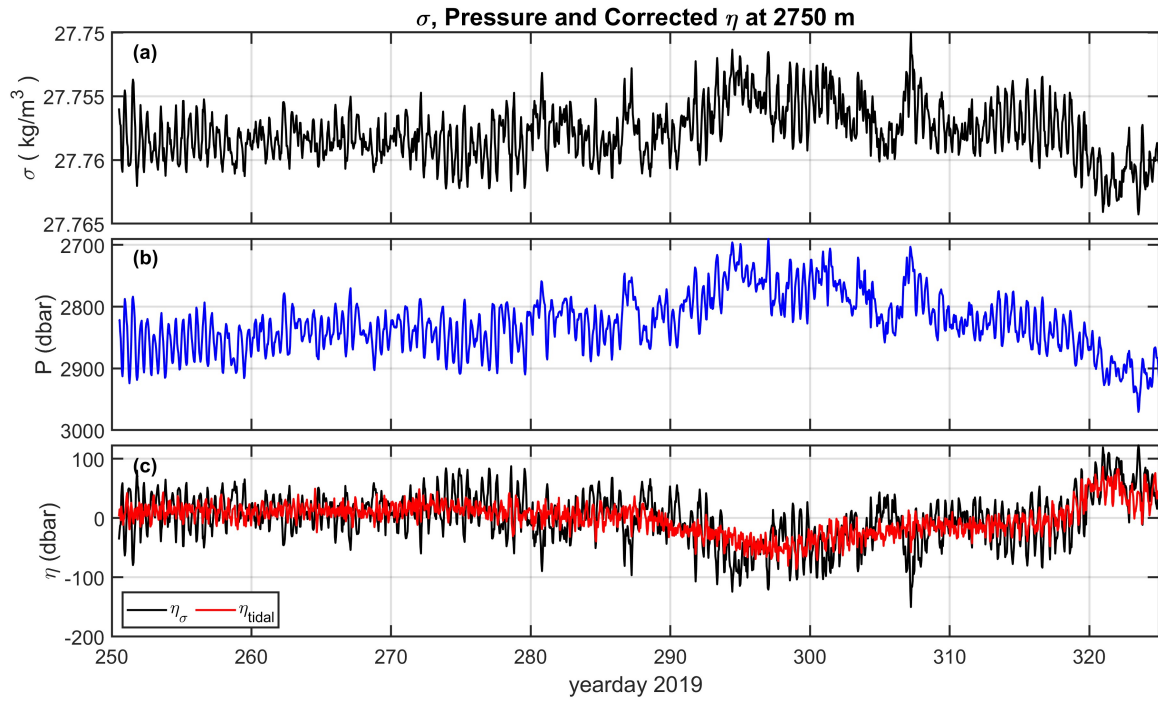**Figure S5.** Same as Figure S4 but only fixed sensors at the south mooring below 500 m.

Figure S6. Time series of (a) the potential density anomaly σ, (b) pressure, and (c) the vertical displacement η of the north mooring at 2750 m. The black line is the total displacement η_σ measured, and the red line is the corrected displacement due to internal tide η_{tide}.
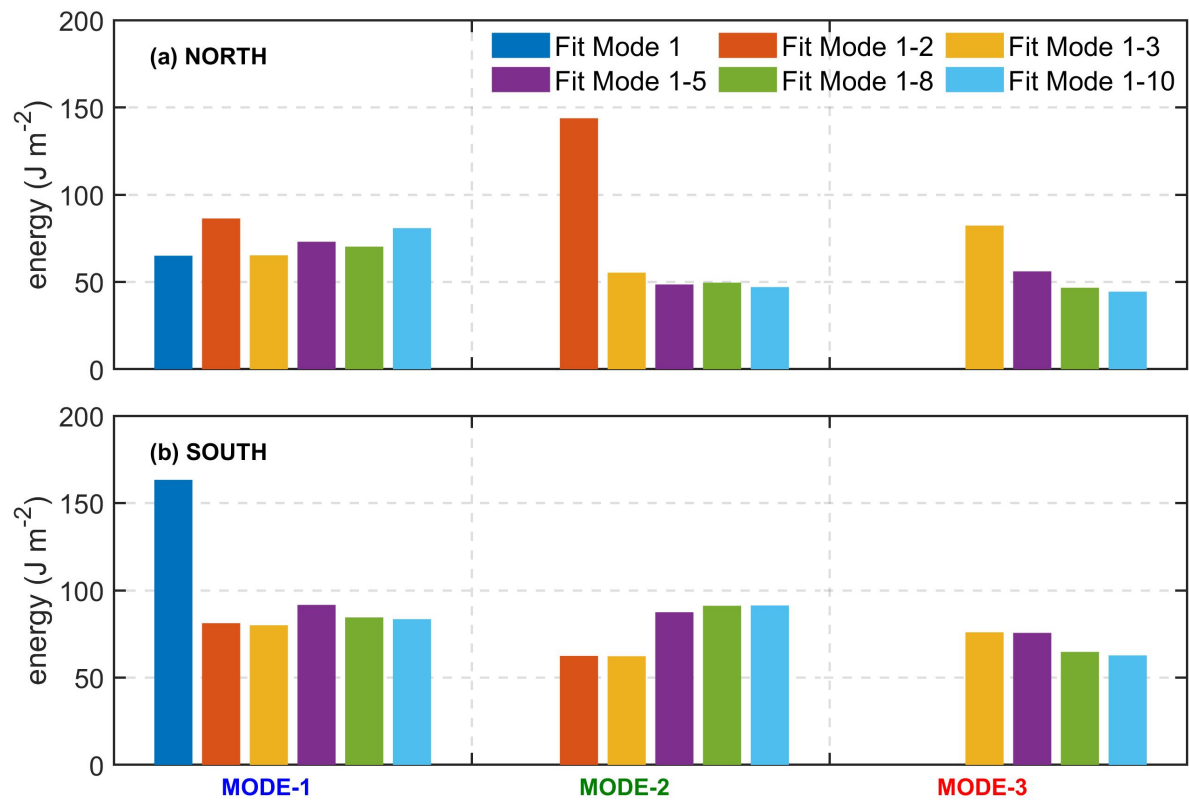
January 6, 2024, 4:43am

Figure S7. Energy of mode 1-3 (x axis) when mode fitting with different mode number at (a) the north mooring and (b) the south mooring. Six scenarios are examined and shown in different color bars; (blue) fitting only mode 1, (orange) fitting mode 1-2, (yellow) fitting mode 1-3, (purple) fitting mode 1-5, (green) fitting mode 1-8 and (blue) fitting mode 1-10.
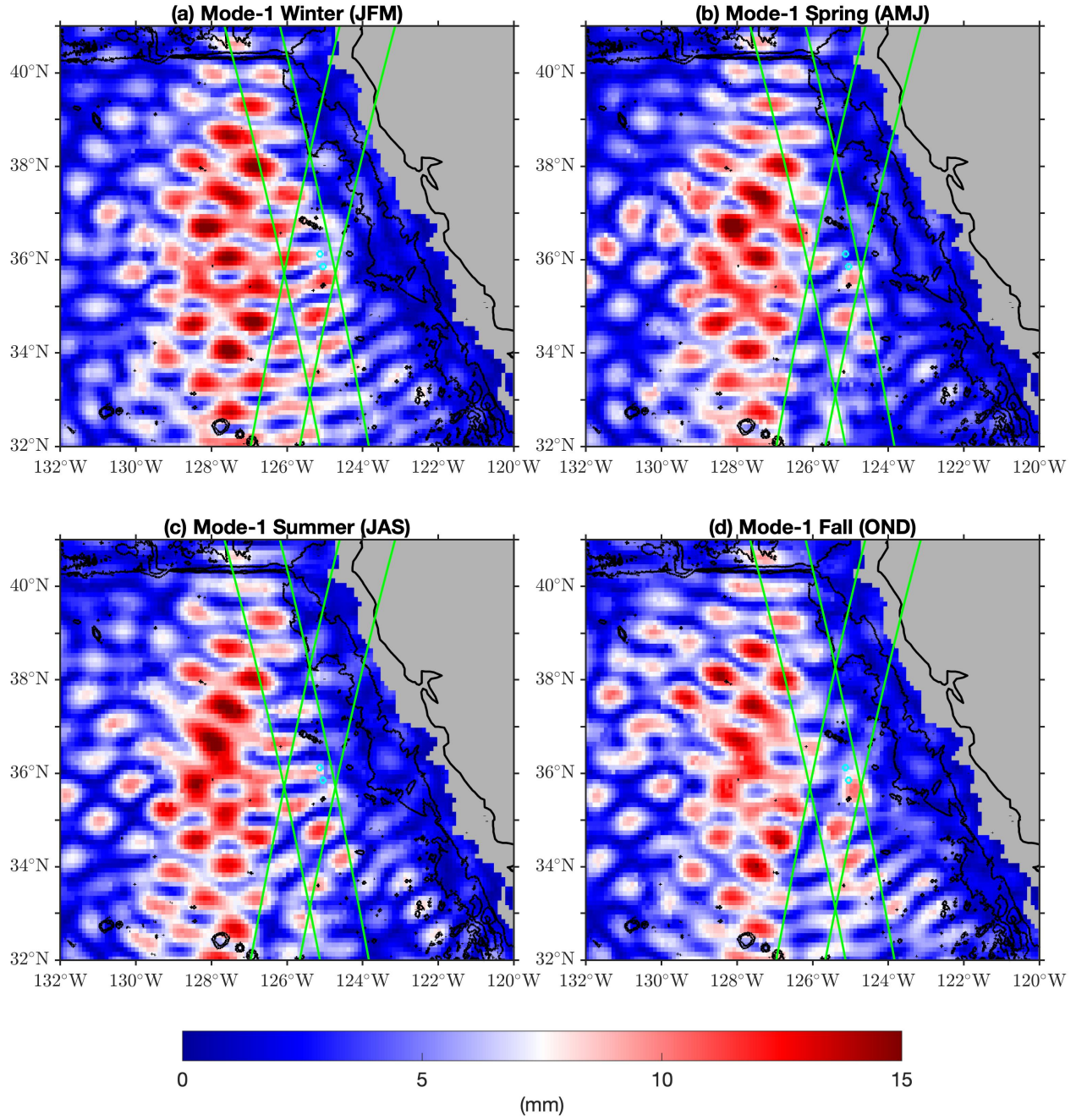
Figure S8. The SSHAs (mm) of mode-1 M_2 internal tides from four climatologically seasonal models. Each seasonal model consists of data from three months: (a) January, February, and March for winter, (b) April, May, and June for spring, (c) July, August, and September for summer, (d) October, November, and December for fall. Green lines are the SWOT Cal/Val swath tracks and cyan circles are the two moorings from the SWOT pre-launch campaign. Contours for the 3000-m and 3800-m isobath are shown.

January 6, 2024, 4:43am